F_K = kinetic force, dynes
F_P = excess pressure force, dynes
F_S = interfacial tension force, dynes
g = acceleration of gravity, 980 cm./sec.^{2}
K = numerical coefficient
l_s = system length parameter, as defined by Equation (4)
N_{We} = Weber number
p, p' = pressure in continuous and dispersed phases, respectively, dynes/sq.cm.
Q = volume flow rate of dispersed phase, cc./sec.
U_J = jetting velocity, cm./sec.
U_N = dispersed phase average velocity through the nozzle, cm./sec.
U_{ri} = average rise velocity of drop over first drop diameter of rise, cm./sec.
$U_{R\infty}$ = steady state rise velocity of drop, cm./sec.
V_F = drop volume, cc.
μ = continuous phase viscosity, g./(cm.)(sec.)
ρ, ρ' = densities of continuous and dispersed phases, respectively, g./cc.
σ = interfacial tension, dyne/cm.

LITERATURE CITED

1. Fujinawa, K., T. Maruyama, and Y. Nakaike, *Kagaku Kikai*, **21**, 194 (1957).
2. Hayes, W. B., B. W. Hardy, and C. D. Holland, *AIChE J.*, **5**, 319 (1959).
3. Hayworth, C. B., and R E. Treybal, *Ind. Eng. Chem.*, **42**, 1174 (1950).
4. Kintner, R. C., private communication (1967).
5. Klee, A. J., and R. E. Treybal, *AIChE J.*, **2**, 244 (1956).
6. Shiffler, D. A., Ph.D. thesis, Cornell Univ., Ithaca, N. Y. (1965).
7. Smith, S. W. J., and H. Moss, *Proc. Roy. Soc. (London)*, **A93**, 373 (1917).
8. Tyler, E., and E. G. Richardson, *Proc. Phys. Soc. (London)*, **37**, 297 (1925).

Manuscript received February 13, 1967; revision received April 26, 1967; paper accepted May 22, 1967.

Kinetics of Physical Adsorption of Propane from Helium on Fixed Beds of Activated Alumina

AUGUSTE E. RIMPEL, JR., DAVID T. CAMP, JOHN A. KOSTECKI, and LAWRENCE N. CANJAR

Carnegie Institute of Technology, Pittsburgh, Pennsylvania

The kinetics of physical adsorption of propane from helium on fixed beds of activated alumina at 30°C. and at atmospheric pressure was studied. Two grades of activated alumina with the same average pore size distribution but different pore size distributions were used. Gas concentration, flow rate, and adsorbent particle size were also varied. The rate of internal diffusion controlled the adsorption process and was best described by Ficks' equation for unsteady state diffusion into a sphere. The internal diffusion appeared to be by a pore diffusion rather than by a surface diffusion mechanism.

The purpose of this research was to investigate the kinetics of an adsorption system in which one component was adsorbed from an inert carrier gas in a fixed-bed system. Once accurate adsorption rate data were obtained, an attempt was made to correlate these data with rate models that have been proposed in the literature. The system used here consists of propane as the adsorbate, helium as the inert carrier gas, and activated alumina as the adsorbent.

THEORY

During the adsorption of a component from a fluid passing through a bed of adsorption particles, the overall rate of adsorption can be a function of any of the following mechanisms: (1) external mass transfer from the bulk fluid phase through the boundary layer around the particle to the exterior surface of the particle; (2) surface reaction or the dynamics of the adsorption process at the fluid-solid surface; (3) fluid phase pore diffusion into the interior of the particle; and (4) solid phase internal diffusion into the interior of the particle. In many cases, only one of these mechanistic steps controls the overall rate of adsorption.

If external mass transfer is the controlling mechanism, the rate of adsorption is described by (*15*)

$$\left(\frac{\partial q}{\partial t}\right)_z = \frac{k_g a_v RT}{\rho_B}(C - C^*) \qquad (1)$$

whereas for the case where surface reaction is the controlling mechanism, it is described by (*12, 13*)

$$\left(\frac{\partial q}{\partial t}\right)_z = k_1 c\,(q_\infty - q) - k_2 q \qquad (2)$$

If internal diffusion is the controlling mechanism, the transfer can be by two different mechanisms. For the case of fluid phase pore diffusion, the transfer rate is described by (*15*)

$$D_p\left(\frac{\partial^2 C_i}{\partial r^2} + \frac{2}{r}\frac{\partial C_i}{\partial r}\right) = \epsilon\frac{\partial C_i}{\partial t} + \rho_B\frac{\partial q_i}{\partial t} \qquad (3)$$

Auguste E. Rimpel, Jr., is at Arthur D. Little, Inc., Cambridge, Massachusetts. Lawrence N. Canjar and David T. Camp are at the University of Detroit, Detroit, Michigan. John A. Kostecki is with Shell Development Company, Emeryville, California.

whereas for the case of adsorbed layer diffusion, it is described by (15)

$$D_s\left(\frac{\partial^2 q_i}{\partial r^2}+\frac{2}{r}\frac{\partial q_i}{\partial r}\right)=\frac{\partial q_i}{\partial t} \tag{4}$$

where the i subscript refers to point conditions in the interior of the adsorbent particle. If both diffusion mechanisms are significant, for the case of linear equilibrium, the transfer rate is described by (8)

$$\frac{D_p+\rho_B\ KD_s}{\epsilon+\rho_B\ K}\left(\frac{\partial^2 q_i}{\partial r^2}+\frac{2}{r}\frac{\partial q_i}{\partial r}\right)=\frac{\partial q_i}{\partial t} \tag{5}$$

All of these internal transfer models are of a diffusional nature. Rate models of a more kinetic nature, similar to the external mass transfer model, have also been postulated. Although it is realized that these models will only be approximations to the more rigorous diffusional model, their advantage is their mathematical simplicity. The following kinetic models have been postulated in the literature (3, 4, 14):

Glueckauf model 1:

$$\left(\frac{\partial q}{\partial t}\right)_z=K_{G1}\ (q^*-q) \tag{6}$$

Glueckauf model 2:

$$\left(\frac{\partial q}{\partial t}\right)_z=K_{G2}\ (q^*-q)+\left(1-\frac{\pi^2}{15}\right)\frac{dq^*}{dt} \tag{7}$$

Vermeulen model:

$$\left(\frac{\partial q}{\partial t}\right)_z=K_{V1}\frac{(q^{*2}-q^2)}{2q} \tag{8}$$

where the rate constants K_{G1}, K_{G2}, and K_{V1} are related to the surface diffusion coefficient D_s in the following way:

$$K_{G1}=\frac{15\,D_s}{b^2} \tag{9}$$

$$K_{G2}=K_{V1}=\frac{\pi^2 D_s}{b^2} \tag{10}$$

EXPERIMENTAL CONDITIONS

The system chosen for this investigation consisted of adsorbing propane from helium on fixed beds of activated alumina. Three levels of propane concentrations were used, 0.84, 2.24, and 4.49 mole %. Grades H-151 and F-1 of Alcoa activated alumina were used. A summary of the physical properties of these two grades of adsorbent is given in Table 1. Although the two grades of adsorbent had approximately the same average pore diameter, they had significantly different pore size distributions. Grade H-151 had a very narrow distribution of pore diameters about its average pore diameter, while the distribution curve for grade F-1 was very broad. Experimental data were taken with three different particle sizes of the grade H-151 adsorbent, 10-12, 12-14, and 14-16 U.S. mesh, but only one particle size, 10-12 U. S. mesh, of the grade F-1 adsorbent. A summary of the experimental conditions used in this study is shown in Table 2.

Experimental Apparatus

The experimental equipment used in this study consisted of cylinders of prepared gas mixtures, the gas feed system, an adsorption vessel containing the adsorbent and measuring elements, a multiposition concentration measuring system with associated programming equipment, a constant-temperature bath, and the necessary piping and valves. A drawing of the experimental apparatus is shown in Figure 1. The adsorption vessel was fed from gas cylinders of helium and prepared mixtures of propane in helium. The gas from the two cylinders was first passed through separate barium oxide desiccators

TABLE 1. PHYSICAL PROPERTIES OF ALCOA ACTIVATED ALUMINA

	Grade F-1	Grade H-151
Pore volume, ml./g.	0.30	0.52
Pore diameter, Å., average	45	40
Pore volume larger than 30 Å. diameter, ml./g.	0.16	0.28
Average size pore in 30 to 90,000 Å. range	600	42
Surface area	210	390

Pore size distribution	Vol. of adsorbent and unfilled pores, ml./g.	Pore radius Å. above which all pores filled with mercury
F-1	0.475	16
	0.48	22
	0.51	80
	0.56	300
	0.595	5,000
	0.63	45,000
H-151	0.39	14
	0.45	17
	0.50	20
	0.56	25
	0.60	30
	0.62	100
	0.65	350
	0.66	700
	0.67	18,000
	0.675	45,000

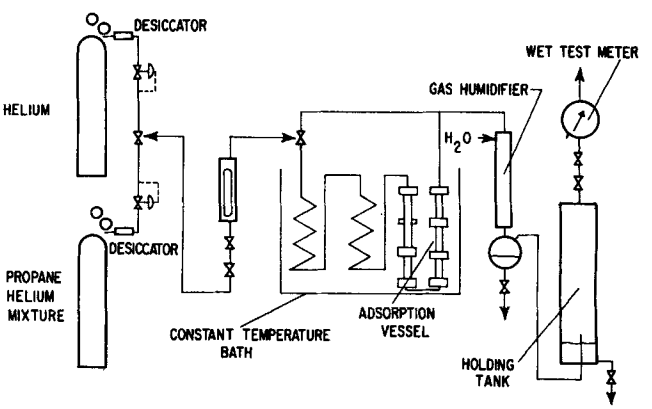

Fig. 1. Piping schematic.

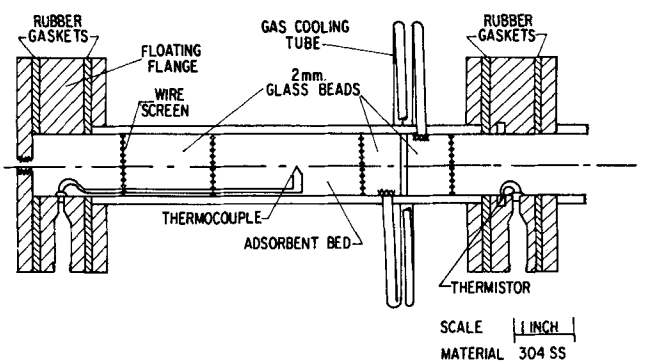

Fig. 2. Adsorption vessel detail.

to remove any trace quantities of water vapor. It then flowed through ¼ in. 304 stainless steel tubing to the gas selector switch, metering valves, a rotometer, and then into the adsorption vessel which was immersed in a constant-temper-

ature bath at 30°C. The gas was heated to the bath temperature by approximately 20 ft. of tubing before entering the adsorption vessel.

The adsorption vessel consisted of five adsorption tubes in a series each made of 1-in. I.D. 304 SS tubing with a wall thickness of ⅛ in. The first adsorption tube was 14 in. long, while the remaining four were each only 7 in. long. The adsorption tubes were connected together by flanges gasketed in ⅛-in. thick Neoprene rubber. Floating flanges, 0.688 in. thick, containing the assorted electrical leads to measure concentration and temperature, were mounted between the adsorption tube flanges as shown in Figure 2. Before the gas left each adsorption tube, it was passed through a 2-ft.-long external cooler made of 3/16-in. O.D. stainless steel tubing to remove any possible heat of adsorption. It then passed through a gas humidifier column and a wet-test meter before being finally vented.

Gas concentration measurements were made at the exit of each adsorption tube by using the thermal conductivity principle. Using a pair of thermistors mounted in a groove in the wall of the floating flange as the primary element of a thermal conductivity cell, a Wheatstone bridge circuit was constructed whose output was a measure of gas composition. The location of the thermistors in the groove introduced a dynamic lag in the concentration measurement, but this lag could be represented as a combination of two linear lags, and the raw data were corrected for this effect. A single-point self-balancing recording potentiometer was used to make all output measurements from the Wheatstone bridges. Measurements were programmed with motor driven multicam switches and two pole relays so that a concentration measurement was taken at each measuring position every 10 sec.

During this time, inert helium gas was passed through the adsorption vessel. When the system reached thermal equilibrium, the flow rates of the helium gas and the desired gas mixture were set using the rotometer. A bypass around the adsorption vessel permitted making this adjustment without disturbing the gas in the adsorption vessel. Helium was then passed through the beds at the desired flow rate. When the output readings on the recording potentiometer from the five measuring positions became constant, the gas selector switch was thrown, and the propane-helium mixture was introduced into the adsorption vessel at the same flow rate as the helium gas. At the same time, concentration measurements were begun to be taken at the five bed positions and recorded automatically on the recording potentiometer. The flow rate was measured by incremental timing with the wet-test meter. When the output readings from the five measuring positions leveled out to new constant values, the run was complete and helium gas was introduced into the adsorption vessel to remove the adsorbed propane in preparation for the next run.

It was found that it was not necessary to reactivate the bed after each run since no noticeable decrease in capacity was found after performing many runs. Numerous runs could thus be performed with a given adsorbent at various flow rates and inlet gas mixture compositions. The original data are available from the library at Carnegie Institute of Technology (9).

METHOD OF ANALYSIS

Once experimental data are available in the form of concentration vs. time curves, that is, breakthrough curves at different bed lengths for the given system, there are basically two different approaches that can be used to determine which of the various proposed rate models best correlate the data. These two approaches will be called the *differential* and the *integral* approaches. Before illustrating these two approaches, it is first necessary to write a material balance around a differential volume of a fixed bed. If the following conditions are assumed—constant plug flow, isothermal conditions, negligible radical concentration gradients, and negligible longitudinal diffusion—the following material balance can be derived (7):

Table 2. Experimental Conditions

Adsorbent	Series A & B	Series C	Series D	Series F
Type	H-151	F-1	H-151	H-151
Particle size (U.S. mesh)	10-12	10-12	12-14	14-16
Mean diameter, ft.	0.00603	0.00603	0.00507	0.00427
Bulk density, lb./cu. ft.	49.62	56.12	48.94	48.56
External void fraction	0.339	0.458	0.347	0.352
Adsorbent weights, lb.				
Bed 1	0.2220	0.2583	0.2331	0.2213
Bed 2	0.02228	0.02566	0.02282	0.02282
Bed 3	0.02285	0.02503	0.02280	0.02278
Bed 4	0.02285	0.02554	0.02280	0.02278
Bed 5	0.02280	0.02569	0.02279	0.02275
Adsorbent depths, ft.				
Bed 1	0.821	0.845	0.874	0.836
Bed 2	0.0824	0.0839	0.0856	0.0862
Bed 3	0.0845	0.0819	0.0855	0.0861
Bed 4	0.0845	0.0835	0.0856	0.0861
Bed 5	0.0843	0.0840	0.0855	0.0859
Temperature, °C.				
Constant-temperature bath	29.8	29.8	29.8	29.8
Wet-test meter	27.8	28.2	30.0	23.0
Barometric pressure, Hg	28.81 (series A) 29.14 (series B)	29.16	29.10	28.96

The temperature rise in the adsorbent bed was measured with a copper-constantan thermocouple inserted into the first bed as illustrated in Figure 2. Preliminary measurements indicated, however, that the maximum temperature rise in the bed was less than 2°C., and thus the bed was assumed to be isothermal and no further temperature measurements were made.

Experimental Procedure

After the adsorbent had been activated in an oven, charged into the adsorption tubes, and the tubes connected, the adsorption vessel was placed in the constant temperature bath.

$$F\left(\frac{\partial c}{\partial z}\right)_t + \epsilon A_x\left(\frac{\partial c}{\partial t}\right)_z + A_x\rho_B\left(\frac{\partial q}{\partial t}\right)_z = 0 \qquad (11)$$

The term $(\partial q/\partial t)_z$ represents the overall rate of adsorption.

In applying the integral approach, the different rate models that are proposed to describe the different types of adsorption mechanisms are substituted into the differential material balance, and the equation is integrated. Some type of equilibrium relationship, usually a linear one, must be assumed in order to perform the integration. The breakthrough curves obtained from this integration are then compared with the experimental curves for different experimental conditions to test the applicability of the proposed model. However, since the integration of the differential material balance is quite complicated and must usually be done by numerical techniques, only a limited number of solutions are available for some rate models in the literature, and thus only these assumed rate models can be tested.

The differential approach is an analysis procedure whereby more rate models can be tested. It is not necessary to integrate the differential material balance when using this procedure. The rate of adsorption is instead calculated by evaluating the two partial derivatives in the differential material balance $(\partial c/\partial t)_z$ and $(\partial c/\partial z)_t$ from the experimental breakthrough curves. These two partial derivatives were calculated at the experimental data points along the third breakthrough curve, that is, the one after the third bed section, because the $(\partial c/\partial z)_t$ term could be more accurately evaluated about this curve than any of the other four. Various rate models could then be tested against the rate of adsorption data obtained along the breakthrough curve for different experimental conditions to test their validity. Both this type of analysis and the integral analysis were applied to the experimental data.

Both the integral and differential approaches also require that equilibrium information be known for the adsorption system. This information was obtained from a graphical integration of the area above a breakthrough curve as shown below:

$$q_\infty = \int_0^\infty \frac{F}{W_B}(C_o - C)\, dt \qquad (12)$$

The equilibrium amount adsorbed could also be evaluated from a graphical integration of the area under the adsorption rate vs. time curve obtained from the differential analysis with the following equation:

$$q_\infty = \int_0^\infty \left(\frac{\partial q}{\partial t}\right)_z dt \qquad (13)$$

A comparison of the values obtained for the equilibrium amount adsorbed by these two methods provided an internal consistency test of the experimental data. In most cases, these two values checked within a percentage difference of 3%.

The equilibrium curve determined from this analysis of the system is shown in Figure 3. The isotherm is not linear, but it could be described by the equation for a Langmuir type isotherm:

$$q^* = \frac{K_1 C^*}{1 + K_2 C^*} \qquad (14)$$

where K_1 and K_2 are constants.

The average amount adsorbed q at various points along the breakthrough curve could also be evaluated using Equation (13) if the upper limit of integration is changed to the time corresponding to the given concentration point along the breakthrough curve. All of the above calculations were performed on the Control Data G-20 Computer with GATE as the programming language.

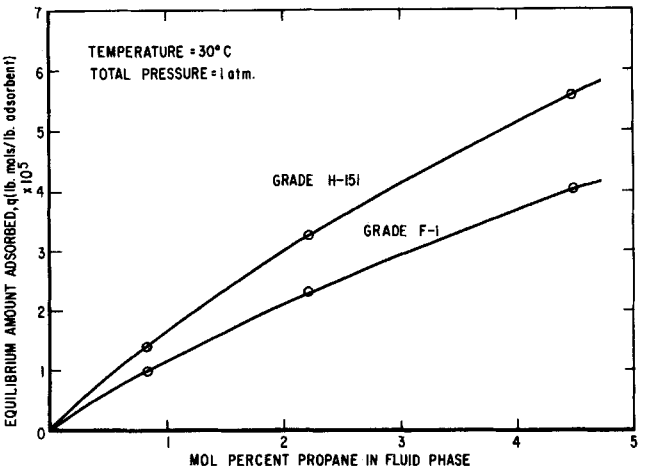

Fig. 3. Equilibrium diagram for adsorption of propane on activated alumina.

RATE MODEL TESTING

The first step in the analysis of the kinetic data was to determine which step, if any, in the overall transfer process was the controlling one. As mentioned previously, the possible controlling steps were external mass transfer, surface reaction, fluid phase internal diffusion, and solid phase internal diffusion.

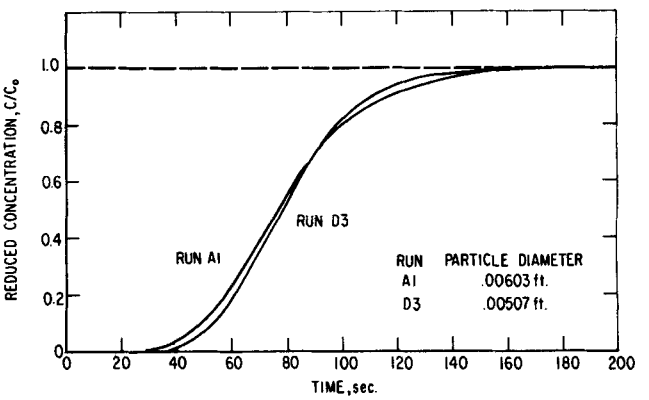

Fig. 4. Breakthrough curves for two runs with only different particle sizes.

Surface reaction was ruled out as the controlling mechanism after the shape of the breakthrough curve, and consequently the rate of adsorption was found to vary with particle size as illustrated in a typical example shown in Figure 4.

With a differential analysis, the external mass transfer coefficients k_g were calculated along the breakthrough curves for all experimental runs. External mass transfer was ruled out as being the controlling mechanism because the values of k_g stayed relatively constant only for runs with diffuse breakthrough curves and they also differed from the values obtained from the existing correlations of Gamson et al. (2) by at least a factor of 10. In addition, the coefficients calculated from runs made at constant Reynolds number with different particles sizes were not the same and the coefficients calculated from similar runs where only the pore size distribution of the adsorbent

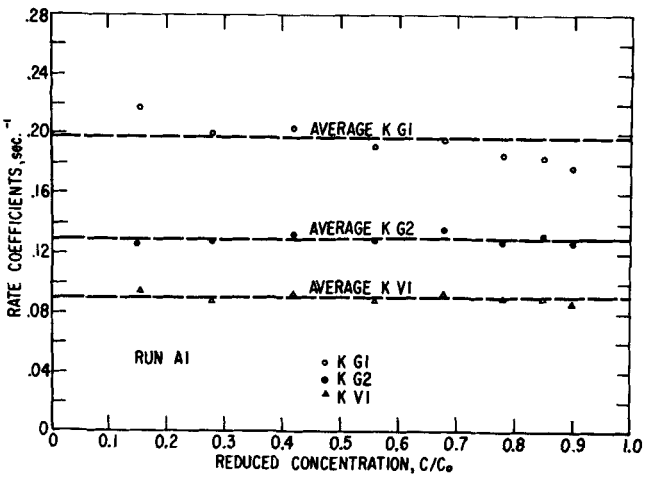

Fig. 5. Kinetic internal diffusion models applied to runs with diffuse breakthrough curves.

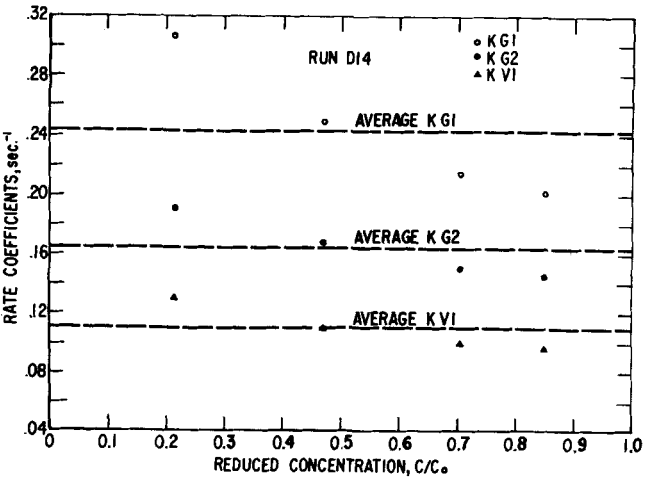

Fig. 6. Kinetic internal diffusion models applied to run with steep breakthrough curve.

particle was changed differed considerably. This evidence did not, however, rule out the possibility of a series mechanism in which external mass transfer played a role.

In evaluating the internal diffusion models, the approximate kinetic types of models that have been previously described were first tested by using a differential analysis. The rate constant of Glueckauf's model 1, K_{G1}, calculated along the breakthrough curve, stayed relatively constant only for runs with diffuse breakthrough curves. There was a significant downward trend in K_{G1} on moving up the breakthrough curve. This trend became more pronounced for runs with steep breakthrough curves to the point where the model could no longer be considered adequate. These observations are illustrated in Figures 5 and 6 where K_{G1} is plotted vs. reduced concentration c/co, for two typical runs with diffuse and steep breakthrough curves. Glueckauf's model 2 and Vermeulen's model were superior to Glueckauf's model 1 in representing the data by reducing or eliminating the decreasing trend in the rate constants as illustrated in the same figures. The rate constants obtained from all these approximate kinetic models, however, showed an increasing trend with flow rate. Since no internal transfer mechanism should be a function of flow rate, this velocity affect was attributed to either the presence of some external mass transfer resistance or to the inadequacy of the proposed models to take into account the different internal gradients within the adsorbent particle.

If external mass transfer resistance is significant, its effect is usually important only in the initial portions of the breakthrough curve for reduced concentrations less than 0.50 (*1*). Thus, if internal transfer coefficients were calculated only from the upper portion of the breakthrough curves where external mass transfer resistance is negligible, these values should not show any velocity effects. A comparison of these calculated values showed that the velocity effect still existed, and thus, this effect was attributed to the inadequacy of the kinetic models.

Glueckauf's model 1 was also tested by using an integral approach with the solution of Hiester and Vermeulen (*6*). Although the same approximate values were obtained for the rate constant, an exact fit could not be made between the experimental and theoretical solution curve over the entire reduced concentration range. It was thus not possible to isolate the velocity effect on the rate constants. No integrated solutions are available for the other two kinetic models.

The diffusional models described by Ficks' equation for unsteady state diffusion into a sphere are more accurately tested by using an integral rather than a differential approach. Rosen (*10, 11*) integrated the differential material balance for the case of linear equilibrium, assuming that internal diffusion is described by an equation of the form of Equation (4). He uses an effective diffusion coefficient which can be interpreted to include, however, both the effects of pore and surface diffusion. Rosen's solution actually takes into account the effect of external mass transfer but a limiting case is that when internal mass transfer controls. Since the solution is limited to the case of linear equilibrium, it could only be applied to the 0.84 mole % propane data where it was possible to approximate the equilibrium curve by a straight line.

On comparing the experimental breakthrough curves data with curves generated from Rosen's solution, an exact fit could be made over the entire reduced concentration range for most runs. The values obtained for the effective diffusion coefficient from Rosen's solution were also not a function of flow rate. These values are illustrated in Table 3. The average value of the effective diffusion coefficient was 13.8×10^{-8} sq.ft./sec. for the grade H-151 adsorbent and 58.1×10^{-8} sq.ft./sec. for the grade F-1 adsorbent.

It was now of interest to examine the numerical magnitude of the effective diffusivity in terms of the contributions from the surface and pore diffusion coefficients. For the case of linear equilibrium, a comparison of Equations (4) and (5) shows these two equations to be equivalent

Table 3. Effective Diffusion Coefficients from Rosen's Solution for 0.84% Propane Mixture

Flow rate at 30°C., 1 atm., cu. ft./sec.	$D'_s \times 10^8$, sq ft./sec.
0.001572	14.3
0.001937	13.0
0.002573	14.0
0.002782	13.3
0.003639	13.6
0.001637	59.3
0.001957	54.2
0.002732	60.9
0.001904	12.0
0.002005	12.3
0.002736	13.2
0.003511	12.7
0.001708	15.2
0.001708	15.1
0.002072	15.4
0.002766	15.3

if

$$D_s' = \frac{D_p + \rho_B K D_s}{\epsilon + \rho_B K} \tag{15}$$

Since in this work, $\epsilon << \rho_B K$, it follows that

$$D_s' = \frac{D_p}{\rho_B K} + D_s \tag{16}$$

For the case of the grade H-151 adsorbent with the narrow distribution of pore sizes about its average pore diameter of 40 Å., the pore diffusion mechanism could be assumed to be by Knudsen diffusion. On calculating the Knudsen diffusion coefficient for the system and substituting this value into Equation (16), we found that the value of $D_p/\rho_B K$ was essentially equal to the value of the effective diffusion coefficient obtained from Rosen's solution. This suggested that the predominant internal transfer mechanism was by pore diffusion rather than by surface diffusion.

It is realized at this point that a critical assumption in the derivation of Equation (16), which separates the effective diffusion coefficient into its pore and surface diffusion contributions, is that equilibrium exists at all times between the surface and fluid concentration in the pores of the particle. Since the average pore diameter of the adsorbent is of the order of 40 Å., it may no longer be possible to apply the results of gross macroscopic equilibrium to this molecular scale. For this reason, the above separation of the effective diffusion coefficient into its surface and pore diffusion contributions may not be accurate. The correlation of the data in terms of the effective diffusion coefficient avoids this problem.

Since a general integral solution for the Fick diffusional model for curved equilibrium was not available at the time of this research work, the experimental data obtained at the two higher propane concentrations could not be tested. A recent publication, however, has presented such a solution for a range of Langmuir isotherms by stepwise numerical computations on a digital computer (8).

CONCLUSIONS

The adsorption of propane from helium on fixed beds of activated alumina under the conditions of this work is controlled by the internal mass transfer of molecules from the external surface of the adsorbent particle into the interior of the particle. Glueckauf's model 1, an approximate kinetic model proposed in the literature, represents the data for runs only when the breakthrough curves are not steep. Glueckauf's model 2 and Vermeulen's model are superior to Glueckauf's model 1 in representing the data, but all these models have rate coefficients that are functions of flow rate, and thus do not adequately describe the experimental data. The data is best correlated by using the integrated solution of Rosen, which assumes that the internal mass transfer rate is described by Ficks' equation for unsteady state diffusion into a sphere. The effective diffusion coefficient is not a function of flow rate and was calculated to be 13.8×10^{-8} sq.ft./sec. for the grade H-151 Alcoa activated alumina and 58.1×10^{-8} sq.ft./sec. for the grade F-1. The predominant internal transfer mechanism appears to be by pore diffusion rather than by surface diffusion.

ACKNOWLEDGMENT

This research was supported by a grant from the National Science Foundation. Grateful acknowledgment is hereby made to this foundation.

NOTATION

a_v = adsorbent bed mass transfer area per unit volume of bed, sq.ft./cu.ft.
A_x = cross-sectional area of bed, sq.ft.
b = particle radius, ft.
c = gas phase concentration, lb.-moles adsorbate/cu.ft.
c_o = inlet gas concentration, lb.-moles adsorbate/cu.ft.
c^* = gas concentration in equilibrium with the adsorbate at the external surface of the adsorbent particle, lb.-moles/cu.ft.
D_p = pore diffusion coefficient, sq.ft./sec.
D_s = surface diffusion coefficient, sq.ft./sec.
D_s' = effective diffusion coefficient, sq.ft./sec.
F = volumetric flow rate of gas through bed, cu.ft./sec.
K = effective equilibrium constant, q^*/c^*, cu.ft./lb. adsorbent
K_1 = constant, Equation (14), cu.ft./lb.
K_2 = constant, Equation (14), cu.ft./lb.-mole
k_1 = rate constant, Equation (2), cu.ft./(lb.-mole)(sec.)
k_2 = rate constant, Equation (2), $sec.^{-1}$
k_g = external mass transfer coefficient, lb.-mole/(sq. ft.)(sec.)(atm.)
K_{G1} = rate constant, Glueckauf's model 1, $sec.^{-1}$
K_{G2} = rate constant, Glueckauf's model 2, $sec.^{-1}$
K_{V1} = rate constant, Vermeulen's model, $sec.^{-1}$
q = average adsorbate concentration on particle, lb.-moles/lb. adsorbent
q^* = adsorbate concentration on particle in equilibrium with adsorbate gas phase concentration at interface, lb.-moles/lb. adsorbent
q_∞ = adsorbate concentration in equilibrium with c_o, lb.-moles/lb. adsorbent
r = distance from center of adsorbent particle, ft.
R = gas constant, (cu.ft.)(atm.)/(lb.-mole)(°R.)
t = time, sec.
T = temperature, °R.
W_B = weight of adsorbent bed, lb.
z = bed depth, ft.

Greek Letters

ϵ = external void fraction, cu.ft. void/cu.ft. bed
ρ_B = bulk density, lb. adsorbent/cu.ft. bed

LITERATURE CITED

1. Carter, J. W., *Brit. Chem. Eng.*, **5**, 625 (1960).
2. Gamson, B. W., George Thodos, and O. A. Hougen, *Trans. Am. Inst. Chem. Engrs.*, **39**, 1 (1943).
3. Glueckauf, E., and J. Coates, *J. Chem. Soc. London*, **149**, 1315 (1947).
4. Glueckauf, E., *Trans. Faraday Soc.*, **51**, 1540 (1955).
5. Hall, K. R., L. C. Eagleton, Andreas Acrivos, and Theodore Vermeulen, *Ind. Eng. Chem. Fundamentals*, **5**, 212 (1966).
6. Hiester, N. K., and Theodore Vermeulen, *Chem. Eng. Progr.*, **48**, 505 (1952).
7. Klotz, I. M., *Chem. Rev.*, **39**, 241 (1946).
8. Masamune, Shinobu, and J. M. Smith, *A.I.Ch.E. J.*, **10**, 246 (1964).
9. Rimpel, A. E., Ph.D. dissertation, Carnegie Inst. Technol., Pittsburgh, Pa. (1964).
10. Rosen, *J. B., J. Chem. Phys.*, **20**, 387 (1952).
11. ———, *Ind. Eng. Chem.*, **46**, 1590 (1954).
12. Thomas, H. C., *J. Am. Chem. Soc.*, **66**, 1664 (1944).
13. ———, *Ann. N. Y. Acad. Sci.*, **49**, 161 (1948).
14. Vermeulen, Theodore, *Ind. Eng. Chem.*, **45**, 1669 (1953).
15. ———, in "Advances in Chemical Engineering," T. B. Drew, and J. W. Hoopes, ed., Vol. II, Academic Press, New York (1958).

Manuscript received January 2, 1966; revision received January 13, 1967; paper accepted January 16, 1967.